Self-consistent one dimension in space and three dimension in velocity kinetic trajectory simulation model of magnetized plasma-wall transition

Roshan Chalise and Raju Khanal

Citation: Physics of Plasmas **22**, 113505 (2015); doi: 10.1063/1.4934601
View online: http://dx.doi.org/10.1063/1.4934601
View Table of Contents: http://scitation.aip.org/content/aip/journal/pop/22/11?ver=pdfcov
Published by the AIP Publishing

Self-consistent one dimension in space and three dimension in velocity kinetic trajectory simulation model of magnetized plasma-wall transition

Roshan Chalise[a] and Raju Khanal
Central Department of Physics, Tribhuvan University, Kirtipur, Kathmandu, Nepal

(Received 10 September 2015; accepted 12 October 2015; published online 6 November 2015)

We have developed a self-consistent 1d3v (one dimension in space and three dimension in velocity) Kinetic Trajectory Simulation (KTS) model, which can be used for modeling various situations of interest and yields results of high accuracy. Exact ion trajectories are followed, to calculate along them the ion distribution function, assuming an arbitrary injection ion distribution. The electrons, on the other hand, are assumed to have a cut-off Maxwellian velocity distribution at injection and their density distribution is obtained analytically. Starting from an initial guess, the potential profile is iterated towards the final time-independent self-consistent state. We have used it to study plasma sheath region formed in presence of an oblique magnetic field. Our results agree well with previous works from other models, and hence, we expect our 1d3v KTS model to provide a basis for the studying of all types of magnetized plasmas, yielding more accurate results. © *2015 AIP Publishing LLC*. [http://dx.doi.org/10.1063/1.4934601]

I. INTRODUCTION

The study of plasma wall-interaction is one of the most important problems for nearly all applications and in the experiments of plasma, where plasma is confined to a finite volume. The correlative works both of experiment and theory have been developed widely during the past several years and yet are still not fully understood.[1–8] Because of its particular importance in plasma technology and fusion research, it remains of undiminished or even growing interest and has received considerable attention in recent years.[9–16] The problem of sheath formation is of great importance, where plasma is in contact with a wall, e.g., the electrode problem in gas discharges, Langmuir probes, and plasma-wall transition (PWT) in tokamaks. Plasma-surface interactions can be important on spacecrafts where the electric fields are sometimes strong enough to give rise to arcs, putting on-board instruments in danger, and also important in dusty-plasma environments.[5] The problems of a magnetized plasma boundary have a particular importance in material processing by plasma and plasma confinement in magnetic fusion devices. Thus, importance of the plasma boundary layer in an external magnetic field has drawn much attention in recent years.[8]

By using a different method, there are a number of theoretical papers that mainly focus on the study of magnetized sheath and pre-sheath. At the interface of plasma and any solid surface, there arises an electrostatic pre-sheath, a Debye sheath, and a magnetic pre-sheath, in magnetized plasma. Chodura[1] has shown that when a magnetic field is present at some oblique angle to the solid surface, a magnetic presheath appears just before the Debye sheath, which produces a significant electric field in this region and deduced a theoretical model for sheath formation, viz., Bohm-Chodura plasma sheath criterion. He introduced a new condition to the flow velocity of ions entering the magnetic presheath, constrained to satisfy the Chodura condition, i.e., the ion velocity parallel to the magnetic field must be equal or greater than the sonic velocity.[2] Due to the high mobility of the electrons, the wall potential will adjust itself to be negative with respect to the surrounding plasma. The repulsion of electrons results in the formation of a positive space-charge region known as a sheath, which shields the quasineutral (bulk) plasma from the negative wall. The region extending from the bulk plasma up to the solid surface is referred to as the "PWT" region. A magnetized plasma sheath is responsible for the flow of particles and energy towards the wall which also affects the bulk-plasma behavior, which in turn greatly modifies the absorption, emission, impurities, and all other characteristics in the plasma.[4] It is shown that the width of the plasma sheath is dependent not only on the collision frequencies and the plasma magnetization, but also on the angle of magnetic field orientation. The grain inside the sheath acquires a more positive charge when the magnetic field is perpendicular to the wall in comparison with the parallel-to-the-wall case. The plasma-sheath characteristic is a sensitive function of the ambient magnetic field direction with respect to the wall.[7] The size of the sheath layer decreases with the increase in the angle between the magnetic field and wall.[16]

Most of the models follow the plasma fluid approximation;[1,2,7,8,15] however, kinetic theory can offer a more accurate solution to the sheath problem.[8] Tskhakaya *et al.* develop a 1d3v (1D in space and 3D in velocity) kinetic Particle-in-cell model of the magnetized plasma-wall transition layer, where the charged and neutral particle dynamics and interaction between them are included in a fully self-consistent way.[6]

In this work, we introduce and describe a new self-consistent 1d3v Kinetic Trajectory Simulation (KTS) applicable for studying the magnetized PWT region. The effect of

[a]Email: plasma.roshan@gmail.com

plasma magnetizations on the sheath is examined for different orientations of the magnetic field. The paper is organized as follows: in Section II, we describe the basic principle of KTS, Section III describes our magnetized plasma sheath model, the numerical calculation method is discussed in Section IV, and the results and discussion are presented in Section V.

II. BASIC PRINCIPLE OF KTS

KTS is an iterative method for numerically calculating self-consistent, time independent kinetic plasma states in some given bounded spatial region. The characteristic features of it are that the distribution function of particle species involved is directly calculated by solving the related kinetic equations along the respective collisionless particle trajectory. In order to obtain the distribution function at any point $(\vec{x},\vec{v})$ of the phase-space, we trace the related trajectories of phase-space where the distribution function is known. Here, we assume the electrons and ions velocity distribution function at the sheath edge to be cut-off Maxwellian in such a way that the most important requirement of the presheath-sheath transition is satisfied, i.e., quasineutrality, the sheath-edge singularity condition, continuity of the first three moments of each species, and the kinetic Bohm-Chodura criterion. In the general case of time-dependent, collisional kinetic theory, the species-s velocity distribution function obeys the Boltzmann equation

$$\frac{df^s(\vec{x},\vec{v},t)}{dt} \equiv \left[\frac{\partial}{\partial t} + \vec{v}\cdot\frac{\partial}{\partial \vec{x}} + \vec{a}^s\cdot\frac{\partial}{\partial \vec{v}}\right] f^s(\vec{x},\vec{v},t) = \left(\frac{\partial f^s}{\partial t}\right)_{coll}, \tag{1}$$

with $\vec{a}^s(\vec{x},\vec{v},t) = \frac{q^s}{m^s}\left[\vec{E}(\vec{x},t) + \vec{v}\times\vec{B}(\vec{x},t)\right]$, where $\vec{E}(\vec{x},t)$ and $\vec{B}(\vec{x},t)$ are the macroscopic (i.e., locally averaged) electromagnetic fields, $\vec{a}^s$ is the macroscopic acceleration of species-s particles (i.e., it is acceleration in these fields), and $(\partial f^s/\partial t)_{coll.}$ is the species-s collision term and $s = (electron/ion)$.

The kinetic Boltzmann equation (1) for collisionless cases takes the well-known form of the Vlasov equation

$$\left[\frac{\partial}{\partial t} + \vec{v}\cdot\frac{\partial}{\partial \vec{x}} + \vec{a}^s\cdot\frac{\partial}{\partial \vec{v}}\right] f^s(\vec{x},\vec{v},t) = 0, \tag{2}$$

i.e., $f^s(\vec{x},\vec{v},t) =$ constant. This means that the velocity distribution function is constant for an observer moving along a collisionless trajectory. Hence, the distribution function at every point along the trajectory can be obtained if its value at one point (i.e., at the boundary) is known. Then, the electron and ion densities are given by

$$n^s(\vec{x}) = \int_{-\infty}^{+\infty} d^3v f^s(\vec{x},\vec{v}). \tag{3}$$

The space charge density is defined as

$$\rho(\vec{x}) = \sum_s q^s n^s(\vec{x}). \tag{4}$$

The electrostatic potential $\phi(x)$ is to be found from Poisson's equation

$$\frac{d^2\phi(\vec{x})}{dx^2} = -\frac{\rho(\vec{x})}{\varepsilon_0}, \tag{5}$$

and the electric field is given by

$$E(\vec{x}) = -\frac{d\phi(\vec{x})}{dx}. \tag{6}$$

In our simulation, we solve Equations (1)–(6) along the collisionless trajectories for given boundary/initial conditions.

III. THE MAGNETIZED PLASMA SHEATH MODEL

In the present work, we restrict ourselves to time independent–collisionless problems, as is appropriate for the sheath regions. The *1d3v* model of magnetized plasma sheath is shown schematically in Figure 1.

The region of interest or simulation region considered is bounded by two parallel planes situated at $x = 0$ and $x = L$, and the plasma consists of only electrons and singly charged ions. We have specified $x = L$ as the "sheath entrance" which separates the non-neutral, collisionless sheath region $(x < L)$ from the quasineutral collisional presheath region $(x > L)$. Similarly, an absorbing wall is specified at $x = 0$. The magnetic field lies in the x-y plane such that

$$\vec{B} = B_0[\cos\theta\hat{x} + \sin\theta\hat{y}]. \tag{7}$$

We assume the plasma particles (electrons and ions) enter the simulation region from the sheath entrance with cut-off Maxwellian velocity distribution functions, the wall does not emit any particles and that both boundaries are perfectly absorbing. Accordingly, the electron velocity distribution function is given by

$$f^e(x,v) = A^e \exp\left[-\left(\frac{v_x^2 + v_y^2 + v_z^2}{v_{tf}^{e\,2}}\right) + \frac{e\varphi(x)}{kT^e}\right] \times \Theta\left[v_{cL}^e(x) - v_x\right], \tag{8}$$

where $v_c^e(x) = \sqrt{\frac{2e[\phi(x)-\phi_0]}{m^e}}$ is the electron cut-off velocity at x, k is the Boltzmann constant, $\phi(x=0) = \phi_0$ is potential at the wall, and $\Theta(x)$ is the Heaviside function, i.e.,

$$\begin{aligned} \Theta(x) &= 1 \quad \text{if } x \geq 0 \\ &= 0 \quad \text{otherwise.} \end{aligned} \tag{9}$$

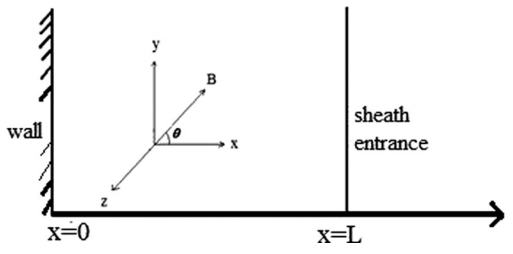

FIG. 1. Schematic magnetized plasma sheath model.

The ion velocity distribution function at $x=L$ is given by

$$f^i(L,v)=A^i\exp\left[-\left(\frac{\left(v_x-v^i_{mL}\right)^2+{v_y}^2+{v_z}^2}{{v^i_{tf}}^2}\right)\right]\ \Theta\left(v^i_{cL}-v_x\right), \tag{10}$$

where $v^s_{tf}=\sqrt{\frac{2k_BT^s}{m^s}}$ is the species-s (ion and electron) thermal velocity, v^i_{mL} is the ion "Maxwellian-maximum" velocity at $x=L$, and $v^i_{cL}(v^i_{cL}<0)$ is the ion cut off velocity at $x=L$.

In the core plasma, the particle distribution would obviously be Maxwellian; however, in the case of sheath formation, the ions are accelerated towards the wall so that they become shifted Maxwellian as given by Equation (10). In addition, for the Bohm criterion to be satisfied by the ions, they must have attained a certain minimum velocity (v^i_{cL}) at the sheath entrance. As the electrons are retracted and reflected by the negative potential wall, their distribution gets cut-off at the sheath entrance as given by Equation (8).

For the velocity distribution given by Equation (8), we can evaluate Equation (3) for electron density at $x=L$ as

$$\begin{aligned}n^e_L&=A^e\int_{-\infty}^{+\infty}dv_x\int_{-\infty}^{+\infty}dv_y\int_{-\infty}^{+\infty}dv_z\exp\left[-\left(\frac{v_x^2+v_y^2+v_z^2}{v^{e^2}_{tf}}\right)\right]\Theta\left(v^e_{cL}-v_x\right)\\&=\frac{A^e{v^{e^3}_{tf}}\pi^{3/2}}{2}C^e,\end{aligned} \tag{11}$$

where

$$C^e=1+\mathrm{erf}(v^e_{cL}/v^e_{tf})=1+\mathrm{erf}\sqrt{\frac{-e\phi_0}{k_BT^e_f}}, \tag{12}$$

"erf" represents the "error function" defined by

$$\mathrm{erf}(x)=\frac{2}{\sqrt{\pi}}\int_0^x d\xi\exp\left(-\xi^2\right). \tag{13}$$

Now, from the velocity distribution function (10) and (3), we get ion density

$$\begin{aligned}n^i_L&=A^i\int_{-\infty}^{+\infty}dv_x\int_{-\infty}^{+\infty}dv_y\int_{-\infty}^{+\infty}dv_z\left[-\left(\frac{\left(v_x-v^i_{mL}\right)^2+v_y^2+v_z^2}{{v^{i^2}_{tf}}}\right)\right]\\&\quad\times\Theta\left(v^i_{cL}-v_x\right)\\&=\frac{A^i\pi^{3/2}{v^{i^3}_{tf}}C^i}{2},\end{aligned} \tag{14}$$

where

$$C^i=1+\mathrm{erf}(\tau^i_{cL}), \tag{15}$$

and

$$\tau^i_{cL}=\left(\frac{v^i_{cL}-v^i_{mL}}{v^i_{tf}}\right). \tag{16}$$

The average velocities for ions can be calculated by using

$$\begin{aligned}u^i_L&=\frac{1}{n^i_l}\int_{-\infty}^{v^i_{cL}}\int_{-\infty}^{+\infty}\int_{-\infty}^{+\infty}\left(v_x\hat{i}+v_y\hat{j}+v_z\hat{k}\right)\\&\quad\times A^i\exp\left[-\left(\frac{\left(v_x-v^i_{mL}\right)^2+v_y^2+v_z^2}{v^{i^2}_{tf}}\right)\right]dv_xdv_ydv_z\\&=\left(v^i_{mL}-\sqrt{\frac{2k_BT^i_f}{\pi m^i}}\frac{D^i}{C^i}\right)\hat{i},\end{aligned} \tag{17}$$

and the average velocity for electrons is

$$\begin{aligned}u^e_L&=\frac{1}{n^e_l}\int_{-\infty}^{v^e_{cL}}\int_{-\infty}^{+\infty}\int_{-\infty}^{+\infty}\left(v_x\hat{i}+v_y\hat{j}+v_z\hat{k}\right)\\&\quad\times A^e\exp\left[-\left(\frac{{v_x}^2+v_y^2+v_z^2}{v^{e^2}_{tf}}\right)\right]dv_xdv_ydv_z\\&=-\sqrt{\frac{2k_BT^e_f}{\pi m^e}}\frac{D^e}{C^e}\hat{i},\end{aligned} \tag{18}$$

where

$$D^i=\exp\left[-(\tau^i_{cL})^2\right], \tag{19}$$

and

$$D^e=\exp\left[-\left(\frac{v^e_{cL}}{v^e_t}\right)^2\right]=\exp\left[\frac{e\Phi_0}{k_BT^e}\right]. \tag{20}$$

The effective temperature for ions is calculated by using

$$\begin{aligned}T^i_{eff,L}&=\frac{m^iA^i}{k_Bn^i_L}\int_{-\infty}^{v^i_{cL}}\int_{-\infty}^{+\infty}\int_{-\infty}^{+\infty}\left(v_x+v_y+v_z-u^i_L\right)^2\\&\quad\times\exp\left[-\left(\frac{\left(v_x-v^i_{mL}\right)^2+v_y^2+v_z^2}{v^{i^2}_{tf}}\right)\right]dv_xdv_ydv_z\\&=T^i_f\left[3-\sqrt{\frac{2m^i}{\pi k_BT^i_f}}\frac{D^i}{C^i}\left(v^i_{cL}-v^i_{mL}\right)-\frac{2}{\pi}\frac{D^{i^2}}{C^{i^2}}\right],\end{aligned} \tag{21}$$

and the effective temperature for electrons as

$$\begin{aligned}T^e_{eff,L}&=\frac{m^eA^e}{k_Bn^e_L}\int_{-\infty}^{v^e_{cL}}\int_{-\infty}^{+\infty}\int_{-\infty}^{+\infty}\left(v_x+v_y+v_z-u^e_L\right)^2\\&\quad\times\exp\left[-\left(\frac{\left({v_x}^2+v_y^2+v_z^2\right)}{v^{ei^2}_{tf}}\right)\right]dv_xdv_ydv_z\\&=T^e_f\left[3-\frac{2}{\sqrt{\pi}}\frac{v^e_{cL}}{v^e_{tf}}\frac{D^e}{C^e}-\frac{2}{\pi}\frac{D^{e^2}}{C^{e^2}}\right].\end{aligned} \tag{22}$$

IV. NUMERICAL METHOD

The "simulation region" lying between $x=0$ and $x=L$ is discretized uniformly in configuration and velocity space.

The position grid point in this region is denoted as $x_j (j = 1, 2, 3, ...n_x)$ with n_x the total number of grid points, and the separation between consecutive grid points is denoted by Δx. In our discretization, $j = 1$ and $j = n_x$ correspond to $x = 0$ and $x = L$, respectively, and we consider n_x to be large enough such that the grid size is always less than the Debye length of the injected electrons. The electron density at grid point x_j is obtained by using the electron distribution function (8) in the expression for particle density (11). In order to obtain the electron density profile, we require $\phi(x)$ to be known. In our calculation, we obtain $\phi(x)$ only at the grid points x_j so that we obtain the electron density at these points in terms of potential as

$$n^e(\phi) = n_L^e \exp\left[\frac{e\phi(x)}{kT_f^e}\right]\left[\frac{1+\text{erf}\sqrt{\frac{e(\phi(x)-\phi_0)}{kT_f^e}}}{1+\text{erf}\sqrt{\frac{-e\phi_0}{kT_f^e}}}\right], \quad (23)$$

where $n_j^e = n_j^e(x_j)$ and $\phi_j = \phi(x_j)$.

Hence, one can obtain the electron density at any point if the potential profile is known.

In the KTS method, we trace the collisionless ion trajectories to calculate the related ion velocity distribution functions along them. For these calculations, we simply discretize the ion equation of motion in a time-centered manner as

$$\frac{x^{m+\frac{1}{2}} - x^{m-\frac{1}{2}}}{\Delta t} = v_x^m, \quad (24)$$

and for change in v_x

$$\frac{v_x^m - v_x^{m-1}}{\Delta t} = \frac{e}{m^i}E\left(x^{m-\frac{1}{2}}\right) - \frac{eB_0 \sin\theta}{m^i} v_z^{m-\frac{1}{2}}. \quad (25)$$

For change in v_y

$$\frac{v_y^m - v_y^{m-1}}{\Delta t} = \frac{eB_0 \cos\theta}{m^i} v_z^{m-\frac{1}{2}}. \quad (26)$$

For change in v_z

$$\frac{v_z^m - v_z^{m-1}}{\Delta t} = \frac{eB_0}{m^i}\left(v_x^{m-\frac{1}{2}}\sin\theta - v_y^{m-\frac{1}{2}}\cos\theta\right), \quad (27)$$

respectively, where Δt is the numerical time-step size, m is an integer such that $m \geq 0$ and the (integral or half integral) superscript, i.e., $v^m = v(t^m)$ and $x^{m+\frac{1}{2}} = x\left(t^{m+\frac{1}{2}}\right)$, and so on. So, $m = 0$ corresponds to t^0 which is equal to 0 with the injection (or starting) values $x^0 = L$ and $v_x^0 = v_{\tau L}^i$. The choice of positions at half integral times and velocity at integral times in Equations (24)–(27) makes the numerical scheme time centered. For any time step $m \geq 1$, with $x^{m-\frac{1}{2}}$ and v_x^{m-1} being given from the $(m-1)^{st}$ step.

We calculate the new ion velocity from Equation (25) as

$$v_x^m = v_x^{m-1} + \frac{e\Delta t}{m^i}E\left(x^{m-\frac{1}{2}}\right) - \frac{eB_0\Delta t \sin\theta}{m^i} v_z^{m-\frac{1}{2}}, \quad (28)$$

and we can also find new positions of the ions from Equation (24)

$$x^{m+\frac{1}{2}} = x^{m-\frac{1}{2}} + \Delta t v_x^m.$$

Thus, the numerical scheme ends up with x-points at half-integral times $\left(x^{m+\frac{1}{2}}\right)$ and velocities at integral times (v_x^m) along a collisionless trajectory. We can also find the ion velocity at $x^{m+\frac{1}{2}}$ by the relation $v_x^{m+\frac{1}{2}} = \frac{v_x^m + v_x^{m+1}}{2}$.

The ion density distribution $n^i(x)$ is obtained by integrating the ion velocity distribution function over velocity space. The ion density at x_j, where the distribution functions $f^i(x_j, v_{\tau j}^i)$ and the intersection velocities of all ion trajectories $v_{\tau j}^i$ are given, is obtained by the following discretized form:

$$n^i(L) = \frac{1}{2}\sum_{\tau=1}^{n_{tra}-1}\left[f^i\left(x_j, v^i{}_{\tau j}\right) + f^i(x_j, v_{\tau+1\,,j}^i)\right](v_{\tau+1,j}^i - v_{\tau j}^i). \quad (29)$$

The main iteration scheme, which carries out the m^{th} iteration, i.e., it calculates new distributions $\phi^{(m)}(x_j)$ for a given input (old) potential distribution $\phi^{(m-1)}(x_j)$ by performing the following three steps.

Step 1: The new electron density distribution $n^{e(m)}(x_j)$ is calculated analytically using Equation (23), and new ion density distribution $n^{i(m)}(x_j)$ is calculated by the kinetic approach, using Equation (29).

Step 2: The new space charge density $\rho^{(m)}(x_j)$ is calculated from using the new densities of electrons and ions as obtained in step 1.

Step 3: The new potential distribution $\phi^{(m)}(x_j)$ is calculated numerically using Poisson's equation, with the new space-charge density $\rho^{(m)}(x_j)$.

The exact solution of Poisson's equation converges only for short systems (a few Debye lengths). As the system length increases, small fluctuations of the potential causes unphysical accumulation of the charges and the scheme breaks down. To overcome this difficulty, we use the relaxation scheme.[17] The new potential distribution $\phi_{ex}^{(m)}(x_j)$ is obtained numerically, which is linearly combined with the old potential distribution $\phi^{(m-1)}(x_j)$ to obtain the "re-adjusted" new potential distribution $\phi^{(m)}(x_j)$, which is actually used as the relevant result of the mth iteration

$$\phi^{(m)}(x_j) = w\phi_{ex}^{(m)}(x_j) + (1-w)\phi^{(m-1)}(x_j), \quad (30)$$

where w is relaxation parameter, having with $0 < w < 2$. The new potential distribution $\phi^{(m)}(x_j)$ obtained in step 3 of the main Iteration Block is compared with the old potential distribution $\phi^{(m-1)}(x_j)$, and we consider the convergence to be reached if at each point x_j the condition

$$|\phi^{(m)}(x_j) - \phi^{(m-1)}(x_j)| \leq \delta, \quad (31)$$

with δ defined as accuracy parameter.

V. RESULTS AND DISCUSSION

To demonstrate our model, we consider a simplified magnetized sheath of hydrogen plasma with mass ratio $m_i/m_e = 1836$, plasma density $n = 10^{20}\,m^{-3}$, and temperature $T_i = T_e = 11$ eV for different magnitude and orientation of the magnetic field. The simulation region is considered to be ten times the electron Debye length at the sheath entrance

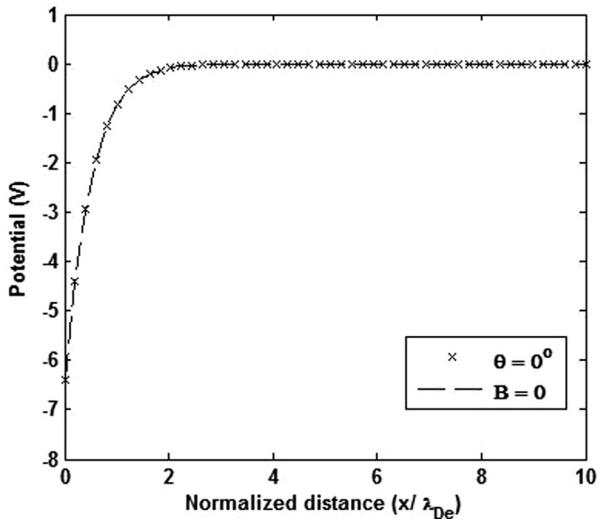

FIG. 2. Potential profile for $\theta = 0^\circ$ and $B = 0$.

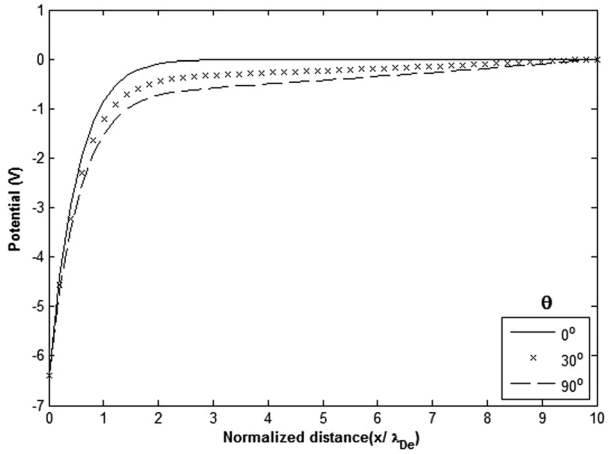

FIG. 3. Potential profile for different angles and $B = 500$ mT.

(λ_{De}), which, for the parameters considered, is much smaller than the ion and electron gyro-radius. The total potential profile in the plasma sheath region as obtained from our KTS simulation for different angles of incidence and strength of the magnetic field is shown in Figures 2–4. In these plots, the distance from the wall is normalized with respect to the electron Debye length at the sheath entrance (λ_{De}). We have seen that the potential profile at the wall dependences is rather weak. It is clearly seen in Figure 2 that when the angle of incidence is $\theta = 0$ or $B = 0$, the dynamics of floating-sheath formation is similar to the one for non-magnetized plasma.[1] For the case of oblique, it has been observed that the magnetized plasma sheath region has two distinct regions: magnetic field dominant region lying close to the sheath entrance and electric field dominant region (almost no effect of magnetic field) lying close to the wall and total electric potential drops between the wall and the plasma sheath.

Figures 3 and 4 clearly indicate that the potential profile consists of two parts: a magnetic field dominant region lying

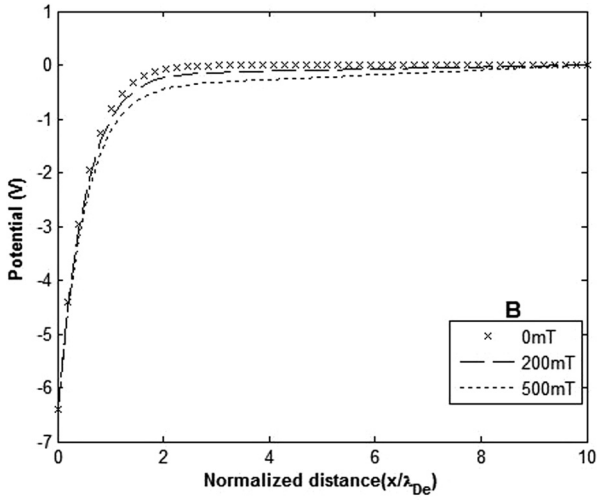

FIG. 4. Potential profile for varying magnetic field with $\theta = 30^\circ$.

close to the sheath entrance and another region lying close to the wall where the effect of magnetic field is negligible.

In this work, we have developed the 1d3v KTS model for studying bounded plasmas and exemplarily applied here to a magnetized hydrogen plasma sheath. This model should act as a first step towards simulating a 3d-magnetized plasma sheath. As our results agree well with earlier works,[1,9,16] we expect our model to work as a basis for studying all types of magnetized plasma sheaths using a kinetic approach. Our results agree well with previous works from other models, and hence, we expect our 1d3v self-consistent KTS model is to provide a basis for studying all types of magnetized plasmas, using the kinetic approach. In future, we envisage extending our model to fully 3-dimensional cases.

[1]R. Chodura, Phys. Fluids **25**(9), 1628 (1982).
[2]K.-U. Riemann, J. Phys. D: Appl. Phys. **24**, 493 (1991).
[3]K.-U. Riemann, Phys. Plasmas **1**(3), 552 (1994).
[4]B. Singha, A. Sarma, and Joyanti Chutia, Phys. Plasmas **9**(2), 683 (2002).
[5]D. D. Tskhakaya, P. K. Shukla, B. Eliasson, and S. Kuhn, Phys. Plasmas **12**, 103503 (2005).
[6]D. Tskhakaya, S. Kuhn, Y. Tomita, K. Matyash, R. Schneider, and F. Taccogna, Contrib. Plasma Phys. **48**, 121 (2008).
[7]B. P. Pandey, A. Samarian, and S. V. Vladimirov, Plasma Phys. Controlled Fusion **50**, 055003 (2008).
[8]M. Khoramabadi, H. Ghomi, and P. K. Shukla, J. Appl. Phys. **109**, 073307 (2011).
[9]R. Chalise and R. Khanal, Plasma Phys. Controlled Fusion **54**, 095006 (2012).
[10]J. P. Sheehan, N. Hershkowitz, I. D. Kaganovich, H. Wang, Y. Raitses, E. V. Barnat, B. R. Weatherford, and D. Sydorenko, Phys. Rev. Lett. **111**, 075002 (2013).
[11]J. Hromadka, T. Ibehej, and R. Hrach, Phys. Scr. **T161**, 014068 (2014).
[12]J. P. Sheehan, I. D. Kaganovich, H. Wang, D. Sydorenko, Y. Raitses, and N. Hershkowitz, Phys. Plasmas **21**, 063502 (2014).
[13]D. D. Tskhakaya, Sr. and L. Kos, Phys. Plasmas **21**, 102115 (2014).
[14]S. Langendorf and M. Walker, Phys. Plasmas **22**, 033515 (2015).
[15]R. Moulick and K. S. Goswami, Phys. Plasmas **22**, 033510 (2015).
[16]R. Chalise and R. Khanal, J Mater. Sci. Eng. A **5**, 41 (2015), available at http://www.davidpublisher.org/index.php/Home/Article/index?id=8676.html.
[17]W. H. Press, S. A. Teukolsky, W. T. Vetterling, and B. P. Flannery, *Numerical Recipes in C* (Cambridge University Press, 2002).